Digital calibration test results for Atacama Large Millimeter/submillimeter Array band 7+8 sideband separating receiver

Franco Curotto,[a,b,*] **Ricardo Finger**,[a] **Takafumi Kojima**,[b] **Kazunori Uemizu**,[b] **Álvaro González**,[b] **Yoshinori Uzawa**,[b] **and Leonardo Bronfman**[a]

[a]Universidad de Chile, Departamento de Astronomía, Santiago, Chile
[b]National Astronomical Observatory of Japan, Mitaka, Japan

Abstract. We present the results of a digital calibration technique applied to an Atacama Large Millimeter/submillimeter Array sideband separating wideband astronomical receiver of 275 to 500 GHz radio frequency (RF) and 3 to 22 GHz intermediate frequency bandwidth. The calibration technique consists of computing the magnitude ratio and the phase difference of the receiver output, and then applying correction constants to the digitized signals. Two analog-digital converters are used to digitize the signals and an field-programmable gate array for the processing. No modification in the analog receiver is required to apply the calibration, as it works directly on upper sideband/lower sideband signals. The technique improved the receiver temperature compared with the double sideband case by increasing the sideband rejection ratio by around 30 dB on average. It is shown that even more rejection can be obtained with more careful control of the RF calibration input power. [DOI: 10.1117/1.JATIS.8.2.024004]

Keywords: astronomy; receivers; telescopes; digital processing.

Paper 21143G received Nov. 9, 2021; accepted for publication Jun. 3, 2022; published online Jun. 23, 2022.

1 Introduction

One of the most desired characteristics for astronomical receivers is to have increasingly wider bandwidths both at radio frequency (RF) and intermediate frequency (IF). For example, the Atacama Large Millimeter/submillimeter Array (ALMA) telescope bandwidth is currently divided into 10 bands that are observed by separated receivers. However, recent advancement in technology has made possible the construction of receivers able to process more than one ALMA band at the same time, e.g., band 7 + band 8[1] and band 2 + band 3.[2] (In this paper, we use the ALMA specific definition of bands: band 7 = 275–373 GHz and band 8 = 385–500 GHz.)

On the other hand, with the noise temperature of superconductor-insulator-superconductor (SIS) receivers reaching two to four times the quantum noise level, atmospheric noise is now the main contributor to system temperature at RF.[3,4] Single sideband (SSB) receivers reject the image band produced by down-conversion, reducing the atmospheric noise coming from the image side, at the expense of discarding half of the down-converted bandwidth. Conversely, double sideband (DSB) receivers provide both the upper sideband (USB), and the lower sideband (LSB), but adds both sidebands atmospheric noise at the same output.

Sideband separating receivers (2SB) are a popular receiver type due to its ability to separate USB and LSB, while at the same time rejecting, to some degree, the atmospheric noise from the image band. The 2SB topology relies heavily on careful phase shifting of the input signal to separate the USB and the LSB (see Fig. 1).

Any amount of phase or gain mismatch in a 2SB receiver produces a percentage of sideband power to get leaked to the other band due to imperfect signal cancellation. A figure of merit of the receiver is the sideband rejection ratio (SRR); defined as the power ratio at the output between

*Address all correspondence to Franco Curotto, francocurotto@gmail.com

2329-4124/2022/$28.00

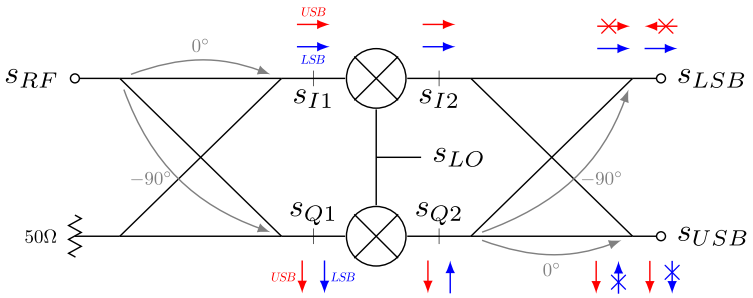

Fig. 1 Diagram of 2SB receiver architecture. Arrows represent phasors for input signals in USB and LSB. Notice how on each output one sideband is maximized, while the other is cancelled out.

a signal coming from the desired band and the rejected band. Theoretically, the SRR can be expressed in terms of the receiver gain and phase imbalances as[5]

$$\mathrm{SRR(dB)} = -10\log_{10}\left(\frac{1-2\sqrt{G}\cos(\phi)+G}{1+2\sqrt{G}\cos(\phi)+G}\right), \tag{1}$$

where G is the power ratio and ϕ is the phase error between the two paths of the rejected sideband. Figure 2 shows the expected SRR for different levels of gain and phase imbalances. It can be seen that, for imbalances of 1 dB in gain and 10 deg in phase one can achieve ∼20 dB of SRR, for 0.1 dB and 1 deg, ∼40 dB, and so on.

Due to the great difficulty of maintaining a consistent gain/phase balance on wideband receivers, specifications for SRR in such receivers are quite modest. As an example, ALMA specifications require that 2SB receivers must have an SRR of at least 10 dB over 90% of its RF bandwidth, and at least 7 dB over the whole bandwidth.[6] Even those moderate requirements have proven to be quite challenging to implement in ALMA receivers. Given that the future plans for ALMA consider the use of receivers covering multiple adjacent bands,[1,7] these requirements will become increasingly more difficult to meet.

Our idea is to apply a digital calibration technique to a wideband receiver, making it possible to significantly improve the SRR. By digitizing the receiver output and using high-speed digital

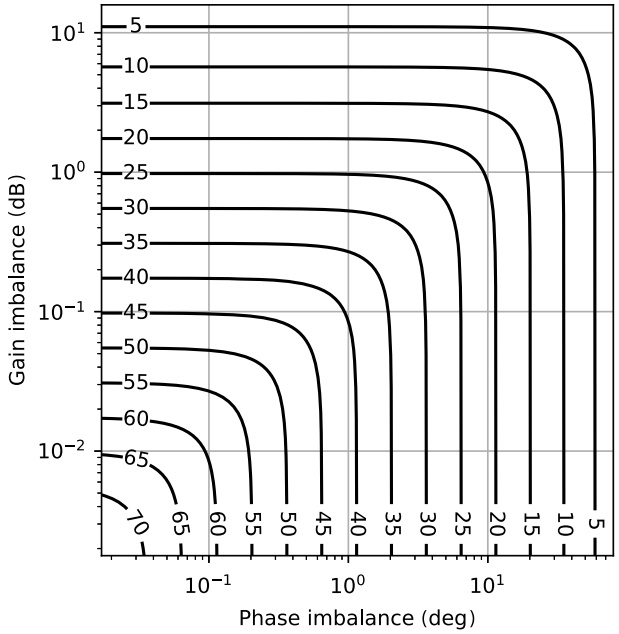

Fig. 2 Contour plots of achievable sideband rejection (in dB) given gain and phase imbalances. Generally, by reducing both the gain and phase imbalances by a factor of 1/10 (dB and degrees, respectively), the SRR improves in 20 dB. This plot is derived from Eq. (1).

signal processors, one can accurately measure the phase and gain mismatch, and apply compensation constants into the signals to achieve far better sideband suppression. The achieved SRR would in turn improves the system temperature to levels comparable to an SSB receiver, while at the same time getting the bandwidth of a DSB receiver. These improvements in receiver performance are key factors to reduce astronomical observation times, and we are convinced they are the way forward for future millimeter-wave receivers.

Previous tests on an ALMA band 9 receiver have shown that digital calibration can achieve SRR of around 40 to 50 dB, which is three to four orders of magnitude of improvement over the uncalibrated case.[8–10] In this experiment, we use the same back-end and calibration procedure as the one from band 9. The novelty of the work is the complexity and state-of-the-art bandwidth of the calibrated receiver. To achieve its wideband characteristics, the receiver must incorporate a waveguide diplexer to accommodate for multiple local oscillators (LO) sources,[11] and a novel wideband SIS mixer that employs a multisection impedance transformer.[1] These additions make for a more complex receiver with more potential points of instability, which in turn is more challenging to calibrate.

In this paper, we report the results of a digital calibration technique applied on a 2SB wideband receiver. The measurement indicates that the technique improves the SRR by 30 dB on average. Further tests show that the method to measure SRR was saturating the receiver, worsening the actual receiver performance. It is proposed that the test can be corrected with better control over the RF calibration input.

The paper is organized as follows: Section 2 describes the calibration method, in Sec. 3 the test setup for the experiment is presented, in Sec. 4 the results of the experiment are shown, Sec. 5 provides discussion on the results, and finally the conclusion of the work is made in Sec. 6.

2 *Digital Calibration Method*

The calibration method consists of measuring the gain ratio and phase difference between both outputs of the receiver at different frequency points and computing a calibration constant to correct for the imbalances. To achieve this, a polyphase filter bank (PFB) based vector analyzer is implemented in hardware using a combination of two high-speed analog-to-digital converters (ADC), and an field-programmable gate array (FPGA). The designed hardware has a bandwidth 1.08 GHz, and a frequency resolution of 527 kHz. (Due to the programmable nature of FPGAs, both resolution and bandwidth could be increased, but it becomes difficult to achieve due to timing and resources constraints of the chip.) At each frequency bin, the gain and phase can be measured as a vector value for both inputs. Then the complex-valued calibration constant $C1/2$ is defined as the ratio of these two values.

A second mode is implemented in the vector analyzer, calibrated mode, where both input signals are combined twice after the PFB. In each combination, one of the signals is digitally multiplied by $-C1/2$ (the negated calibration constant) in the frequency domain (see Fig. 3). Essentially, the constant value is chosen to produce "destructive interference" between the

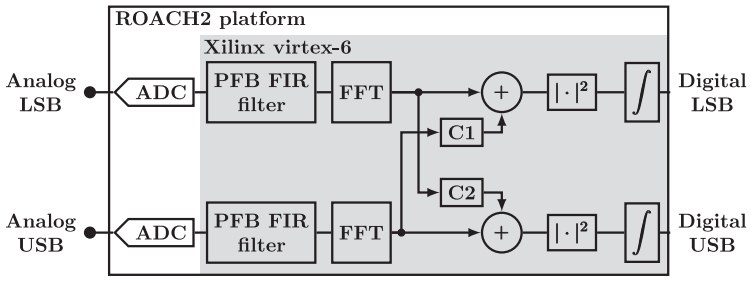

Fig. 3 Diagram of the calibration system implemented in the FPGA. The combination of PFB FIR filter and FFT block form the PFB to convert the signal from the time domain to frequency domain. The $|\cdot|^2$ blocks are square law detectors, and $\int$ blocks are time accumulators, used to reduce noise. To compute the calibration constants memories $C1$ and $C2$ are set to 0. To go to calibrated mode, the calibration constants are loaded to $C1$ and $C2$.

undesired sideband in one output (e.g., the partially rejected LSB signal in the USB output) with the desired sideband of the other output (e.g., the LSB signal of the LSB output).

The steps of the calibration method are the following:

1. An external RF tone (calibration tone) is injected at the receiver input at USB frequency.
2. The calibration tone is swept through the whole USB bandwidth at different frequency points of calibrations. The denser the sweep, the better calibration is achieved in between frequency points (in practice, steps of 1 MHz do not degrade the calibration much in our experience).
3. For each frequency point, the complex-valued calibration constant is computed as

$$C1 = \frac{v_{\mathrm{LSB}}}{v_{\mathrm{USB}}}, \tag{2}$$

   where v_{USB} and v_{LSB} are the measured vector value at USB and LSB outputs, respectively. The calibration constant is then saved to the control computer memory.
4. The hardware is set to calibrated mode, and a second sweep across the USB bandwidth is made.
5. For each frequency point, the negated calibration constant $-C1$ is loaded into the FPGA memory (The loading of the constant can be done into FPGA registers over Ethernet communication. Therefore, no FPGA reprogramming is needed and the time penalty is minimal.), and the digital (calibrated) LSB output is created as $v_{\mathrm{LSB}} - C1 \cdot v_{\mathrm{USB}}$, achieving an improved cancellation of the USB signal at the LSB output.
6. To measure the quality of the calibration, the SRR for LSB is computed.
7. The whole process is repeated for USB bandwidth calibration, injecting an LSB tone, and computing the calibration constant as $C2 = \frac{v_{\mathrm{USB}}}{v_{\mathrm{LSB}}}$.

For a more detailed mathematical justification of the method (see Refs. 10 and 12). To measure SRR after calibration, gain correction formulas must be applied to correct for gain differences between the USB and LSB paths of the receiver, as described in Ref. 13. These formulas are

$$\mathrm{SRR}_{\mathrm{USB}} = M_U \frac{M_L M_{\mathrm{DSB}} - 1}{M_U - M_{\mathrm{DSB}}} \quad \mathrm{SRR}_{\mathrm{LSB}} = M_L \frac{M_U - M_{\mathrm{DSB}}}{M_L M_{\mathrm{DSB}} - 1}, \tag{3}$$

where M_U is the power ratio between USB and LSB output with RF tone at USB input, M_L is the power ratio between LSB and USB output with RF tone at LSB input. M_{DSB} is defined as $\frac{\Delta P_{\mathrm{USB}}}{\Delta P_{\mathrm{LSB}}}$, where ΔP_{USB} and ΔP_{LSB} are defined as the power ratio at USB and LSB output, respectively, when a hot load and a cold load are placed at the input.

Previous implementations of this method[8] require the I/Q signals as inputs of the digital system, meaning that the IF hybrid must be removed from the receiver to apply the calibration. By using the previous algorithm, no component removal is necessary, and instead, the calibration can be performed directly with the USB/LSB outputs. In theory, for a perfectly stable receiver, the achievable SRR is limited by the dynamic range of the digital system. (Inefficiencies in ADCs like integral nonlinearity and jitter, usually affect the digital system dynamic range itself.)

For modern astronomical receivers, the actual SRR after calibration is usually limited by the stability of the receiver, in terms of its ability to maintain a constant phase and gain relation between its outputs over time. If the imbalances of the receiver start oscillating or drifting, the computed constants are no longer valid and the SRR degrades. Common causes for receiver instability at short time ranges (seconds) are high temperature variations, and receiver components operating near saturation point. In practice, it has been observed that, by using this method, SRR can be kept over 40 dB for periods of 24 h in astronomical 2SB receivers.[10]

One possible problem that the method could face is the presence of automatic gain control (AGC) systems, typically used to maintain an optimal power level before the digitizers. The real-time change on AGC gain could lead to variations in the signal phase that would render past calibrations invalid. Possible solutions to this problem are the use of constant-phase AGC circuits,[14] or utilizing high dynamic range digital system to avoid the usage of AGC entirely.

3 *Tests Setup*

3.1 *Receiver Frontend*

The digital calibration method is tested on the 2SB SIS-based Band 7+8 receiver recently developed at National Astronomical Observatory of Japan (NAOJ). The receiver has an RF bandwidth of 275 to 500 GHz, and an IF bandwidth of 3 to 22 GHz. The receiver was designed to meet the ALMA specifications, and it has a mean SRR of ∼10 dB. The RF 90-deg hybrid uses a similar design to the one from the waveguide LO diplexer.[11] The measured amplitude imbalance is <4 dB over 275 to 500 GHz with the worst value at the upper edge of the RF band. The wideband performance of the heterodyne mixer is achieved by the use of an SIS mixer-preamplifier module.[15] Since the preamplifier is integrated in the module and located prior to the IF 90-deg hybrid, the imbalance between two preamplifiers in addition to the SIS mixers affects the receiver SRR. The IF 90-deg hybrid used in this prototype is a commercially available product (Marki Microwave, QH-0226). Note that this component is not optimized for cryogenic purposes. However, the measured amplitude and phase imbalance at cryogenic temperatures were 1 dB typical and 2 dB maximum, and <5 deg, across the 3 to 22 GHz frequency range, respectively. Thus, in this configuration, the imperfections of the gain and phase balances of the analog components, including the RF and IF 90-deg hybrids and two SIS-mixer-preamplifier modules, are the main contributor to the receiver SRR (before digital calibration).

3.2 *Rest of the Test Setup*

A diagram of the test setup is presented in Fig. 4. For the digital calibration system, a ROACH2 platform is used.[16] It consists of two EV8AQ160 ADCs and a Virtex-6 FPGA. The FPGA is programmed to implement two 2048-bin spectrometers with 1.08 GHz of bandwidth (1.08 GHz per sideband). To accommodate the 3 to 22 GHz IF bandwidth of the receiver, a second down-conversion stage is implemented. Signal generators are used to provide the LO signals and the RF tone for the imbalance measurement process. All the input signals have appropriate multiplier chains to achieve the required frequency. For simplicity, the RF tone is kept at a constant power level during the calibration. The RF input can also be switched into a hot-cold load, to implement the gain correction for the SRR computation described in Ref. 13.

4 Results

4.1 *IF Power Level Measurements*

The first round of tests consists in measuring the IF power level at the input of the ADCs, across the full bandwidth. Flatness of IF power is important for the SRR measurement because points of low power will present artificially lower dynamic range when performing the calibration.

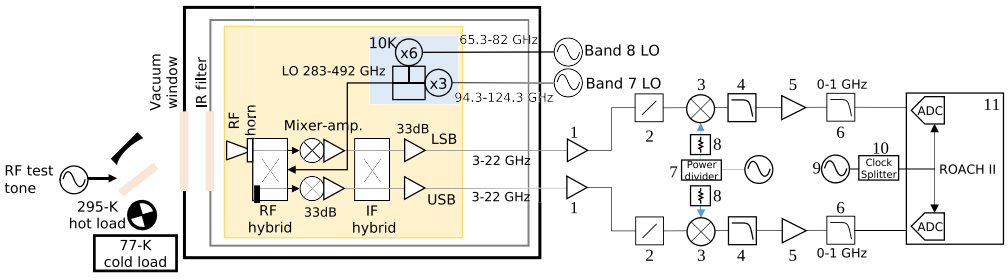

Fig. 4 Setup diagram for the calibration test. The band 7+8 receiver is shown enclosed in the test cryostat. The system between the receiver and the ROACH2 (FPGA platform) is the second down-conversion stage to match the bandwidth of the receiver with that of the digital system. For a detailed description of the components, see Table 3.

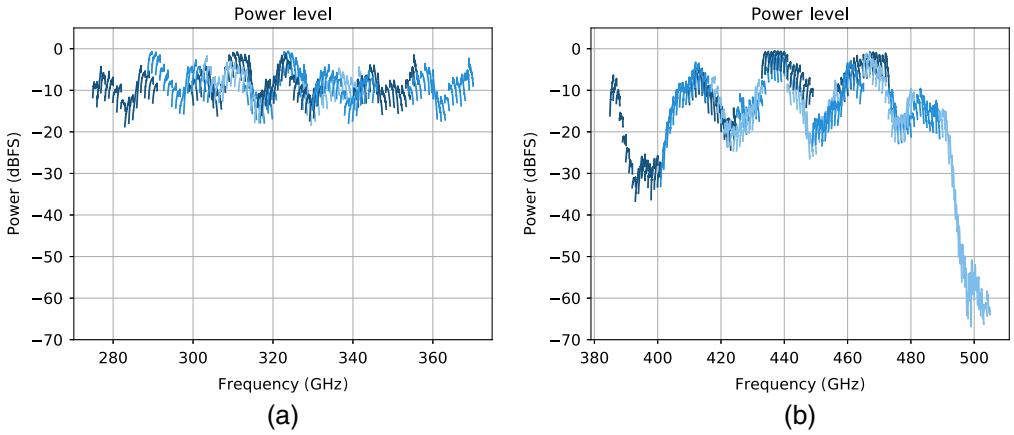

Fig. 5 Results of the measured IF power of the setup. (a) For band 7 and (b) for band 8. Different hues of blue represent different values of LO frequency. The gain is normalized to the digital system full scale. The small 1 GHz variations are due to the gain slope of the second down-conversion stage.

The results are shown in Fig. 5. The experiment requires measuring bands 7 and 8 separately, as the RF test tone source must be changed in the setup for each band. The setup presents variations in IF power of ∼20 dB on band 7 and ∼38 dB on band 8. The IF output power is reasonably flat across the band 7 frequencies, while a relatively large ripple with a period of 20 GHz can be seen in the band 8 frequency range. In addition, significant degradation of the IF output power was identified at the higher edge of band 8. These characteristics are due to the output power of the RF source used at band 8, because of the impedance matching between waveguide components such as multipliers, and RF bandwidth of the final ×6 multiplier. The digital system has a dynamic range of 70 dB, so it will be able to measure SRR values of at least 40 dB, even in the parts of worse ripples, around 395 GHz.

4.2 *SRR Measurements*

The SRR of the receiver is measured both as purely analog (uncalibrated) and after digital calibration (we call the later digital SRR). The results are shown in Fig. 6. The mean values of the SRR for each band are presented in Table 1. The SRR improved by 34 dB for band 7 and 28 dB for band 8, achieving three orders of magnitude improvement in SRR on average.

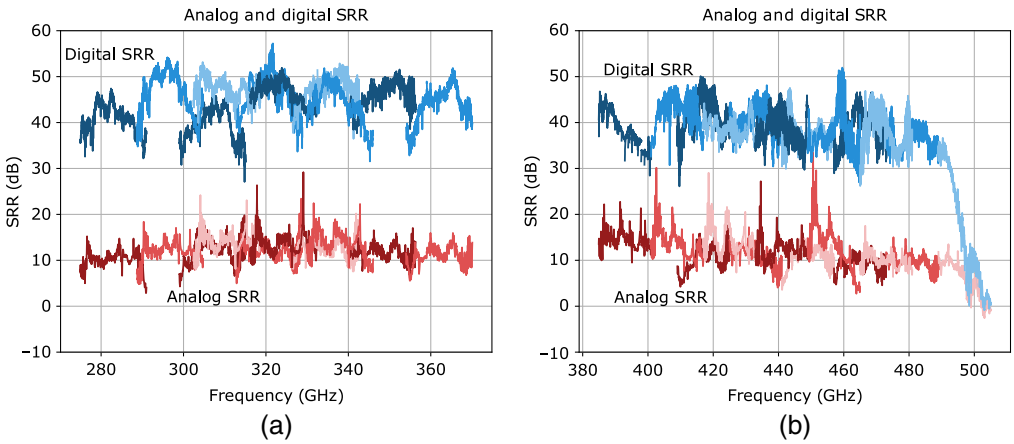

Fig. 6 Results of SRR. (a) For band 7 and (b) for band 8. Hues of red correspond to analog (uncalibrated) SRR, while hues of blue show the digital (calibrated) SRR. In general, SRR decreases at the edges of the IF bands.

Table 1 Mean SRR for each ALMA band. "SRR digital" and "SRR analog" refer to the SRR obtained with and without applying digital calibration respectively.

SRR analog (dB)		SRR digital (dB)	
Band 7	Band 8	Band 7	Band 8
13	13	47	41

Due to the nature of the test setup, at some frequency points, the SRR is computed twice, for two different LO settings (curves of two colors overlapping in Fig. 6). At some parts, the same frequencies have two different values of SRR. That is because, by changing the LO setting, the system gain, saturation point, and stability can change, constraining the SRR differently for each setup.

Even though the increase of SRR is substantial, there are intervals where the digital SRR decreases considerably, especially at the edges of the IF bandwidth. Aside from the drop at 395 GHz, which can be attributable to the gain lost at that frequency, the SRR curves do not significantly correlate with the gain plots from Fig. 5. Therefore, the digital system has sufficient dynamic range and cannot be affecting the SRR measurements at the IF band edges. In the next subsection, the possibility of phase noise, produced by poor stability of the system, is explored as a potential cause of the SRR degradation.

4.3 *Phase Noise Tests*

The first test to measure phase noise in the receiver is to analyze the raw spectra where the calibration tone is set to a frequency with low digital SRR (30 dB). Plots of such spectra for band 7 are shown in Fig. 7, where the tone was set to 303.61 GHz (around 140 MHz at IF). From the plots, the rejected (USB) tone presents large amounts of phase noise around it (high power levels around the test frequency) of about 20 dB over the noise floor. A similar phenomenon occurs for band 8, as shown in Fig. 8, where the rejected tone is present in LSB. In those cases, the phase noise is acting as a higher noise floor that reduces the dynamic range at that specific frequency and limits the calibrated SRR. This behavior is repeated in every case that SRR is substantially low (>35 dB).

A second test is performed to determine if the observed phase noise can be reduced by controlling the calibration tone power. A single frequency with low digital SRR performance is selected (26 dB), and the IF power (at the ADC) and SRR (analog and digital) are recorded

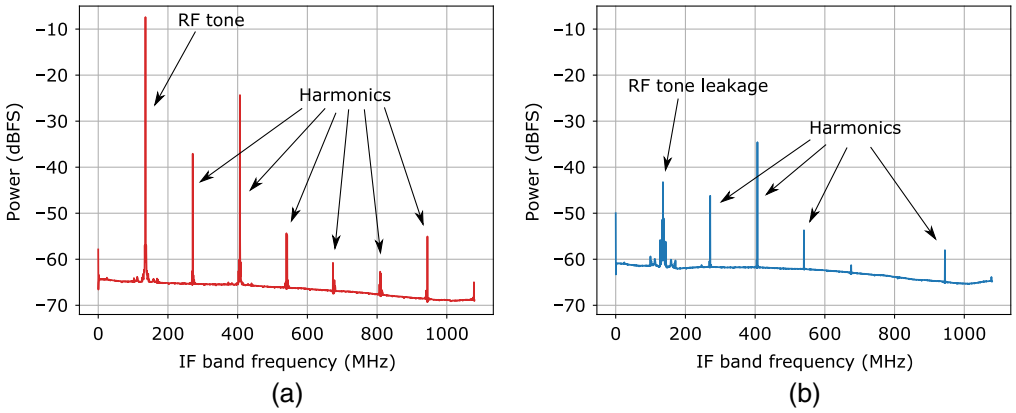

Fig. 7 Raw spectra for a single LO configuration and RF tone. LO: 308.75 GHz, RF: 303.61 GHz (LSB), band 7. (a) Shows the injected RF tone (140 MHz IF) and its harmonics at their legitimate places in the LSB spectrum. (b) Shows the contamination from the RF tone, even after the image suppression, observed in the USB spectrum.

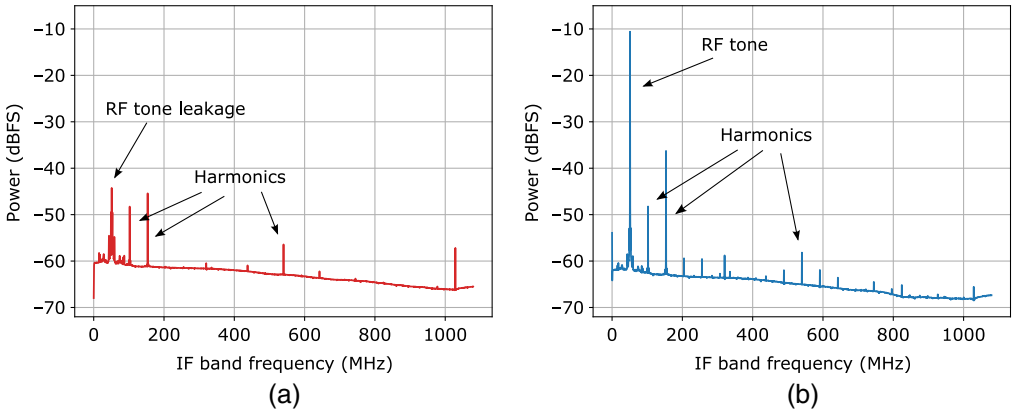

Fig. 8 Raw spectra for a single LO configuration and RF tone. LO: 453 GHz, RF: 457.05 GHz (USB), band 8. (b) Shows the injected RF tone (51 MHz IF) and its harmonics at their legitimate places in the USB spectrum. (a) Shows the contamination from the RF tone, even after the image suppression, observed in the LSB spectrum.

Table 2 Results for the phase noise test performed by modifying the RF power. The IF power and SRR values are the mean over the number of samples. LO: 405 GHz, RF: 409.4 GHz (USB), band 8.

	Power RF (dB)	Power IF (dBFS)	SRR analog (dB)	SRR digital (dB)	Phase noise (dBc/Hz@2.1 MHz)	Samples
Original power	0	−11	4	26	−90	211
Low power	−3	−14	9	32	−94	211

at a rate of one value per second. Additionally, the phase noise is measured as dBc/Hz (decibels relative to the carrier signal, per Hz.) at 2.1 MHz. The 2.1 MHz point is selected because it corresponds to the frequency bin with the highest phase noise level. Then the test is repeated reducing the RF calibration power by −3 dB. The resulting values are shown in Table 2.

From the data, by reducing the RF power, the phase noise was lowered by 4 dB/Hz, and at the same time the analog and digital SRR is increased by 5 and 6 dB, respectively. This behavior suggests that the phase noise in the system is produced by an excess of RF power from the calibration tone, which causes the saturation of one or more of the components at some point of the receiver (Table 3).

5 Discussion

The demonstrated calibration technique has certainly improved the performance of the wideband astronomical receiver, albeit not as expected given the capabilities of the digital system. The SRR measurement method involves injecting a high-power RF tone into the receiver, which is suspected to cause saturation in the RF components, and in turn, the phase noise that limits the achievable SRR. In normal astronomical operation it is unrealistic to expect signals with power 50 dB over the noise floor, making the saturation problem less relevant.

A more realistic SRR measurement can be achieved by fine tuning a specific RF tone power for each calibrated frequency, in particular, reducing the power for points with high phase noise presence, as demonstrated in the last experiment.

To find the appropriate power level, a good approach is to setup a programmable tone sweep that set the RF power to the specific saturation point for each frequency (that can be computed from the plots shown in Fig. 5). Then adjust a wideband IF attenuation, to find the one that maximizes the SRR over the whole bandwidth. With this approach, it is expected to partially improve the calibration at the IF band edges.

Table 3 List of all components used in the second down-conversion stage from the test setup in Fig. 4. The table uses the labels from the figure for easier identification.

#	Component	Product	Manufacturer	Frequency	Spec.
1	Wideband amplifier	ZVA-203GZ+	Mini-circuits	2 to 21 GHz	30 dB
2	Equalizer	MEQ6-26AS	Marki	DC-26 GHz	6 dB@DC, 1 dB@26 GHz
3	Mixer	M8-0326	Marki	RF, LO: 3 to 26 GHz, IF: DC-2 GHz	<7 dB
4	Low pass filter	VLF-1800+	Mini-circuits	DC-1.8 GHz	3 dB@2.125 GHz
5	Medium amplifier	ZKL-2+	Mini-circuits	0.001 to 2 GHz	33.5 dB
6	Low pass filter	VLF-800+	Mini-circuits	DC-0.8 GHz	3 dB@1.075 GHz
7	Power splitter	PD-0150 2-Way	Makri	1 to 50 GHz	3 dB
8	Attenuator			DC-26 GHz	3 dB
9	Synthesizer	5009	Valon Technology	23.5 MHz to 6 GHz	−15 to 15 dBm
10	Power splitter	ZFRSC-183-S+	Mini-circuits	DC-18 GHz	6 dB
11	Signal processor	ROACH2		1.08 GHz	

For the hit in performance in the 490- to 505-GHz band, since it is produced by a dramatic decrease in receiver gain, it is impractical to raise the RF tone power. Instead, improving the gain performance of the RF components is the most reasonable approach.

6 Conclusion

A proof of concept of digital calibration on an ALMA Band 7+8 2SB receiver was successfully tested. The calibration increases the SRR performance of the wideband receiver by 30 dB on average. By additional tests, it was proven that the SRR measurements are actually limited by phase noise present in the output signal, due to receiver saturation. A procedure is described to improve the test results, which involves more careful control over the power of the calibration tone. More generally, these experiments show how digital technology can enhance the observation capabilities of radio telescopes, by being combined in a more direct way with analog receivers.

Acknowledgements

The authors would like to express their gratitude to S. Asayama for helpful discussion. NAOJ acknowledges the support of Japan Society for the Promotion of Science KAKENHI under Grant 18H03725. UChile acknowledges the support of ANID under grants ALMA-ANID 31180005 and Basal Projects ACE210002 and FB210003.

References

1. T. Kojima et al., "275–500-GHz wideband waveguide SIS mixers," *IEEE Trans. Terahertz Sci. Technol.* **8**(6), 638–646 (2018).
2. P. Yagoubov et al., "Wideband 67-116 GHz receiver development for ALMA Band 2," *Astron. Astrophys.* **634**, A46 (2020).
3. A. R. Kerr, S. K. Pan, and H. G. LeDuc, "An integrated sideband separating SIS mixer for 200–280 GHz," in *Proc. Ninth Int. Symp. Space Terahertz Technol.*, pp. 215–221 (1998).

4. P. R. Jewell and J. G. Mangum, "System temperatures, single versus double sideband operation, and optimum receiver performance," *Int. J. Infrared Millimeter Waves* **20**(2), 171–191 (1999).
5. J. W. Kooi, "Advanced receivers for submillimeter and far infrared astronomy," English PhD thesis, University of Groningen (2008).
6. C. T. Cunningham et al. "Front-end sub-system for the 12 m antenna array technical specifications," in Atacama Large Millimeter Array Internal Technical Document (2007).
7. T. Mroczkowski et al., "Wide bandwidth considerations for ALMA band 2," https://arxiv.org/abs/1905.09064 (2019).
8. R. Rodríguez et al., "A sideband-separating receiver with a calibrated digital if-hybrid spectrometer for the millimeter band," *Publ. Astron. Soc. Pac.* **126**(938), 380 (2014).
9. R. Finger et al., "Ultra-pure digital sideband separation at sub-millimeter wavelengths," *Astron. Astrophys.* **584**, A3 (2015).
10. R. Rodríguez et al., "Digital compensation of the sideband-rejection ratio in a fully analog 2SB sub-millimeter receiver," *Astron. Astrophys.* **619**, A153 (2018).
11. A. Gonzalez et al., "275–500 GHz waveguide diplexer to combine local oscillators for different frequency bands," *IEEE Trans. Terahertz Sci. Technol.* **7**(6), 669–676 (2017).
12. M. A. Morgan and J. R. Fisher, "Experiments with calibrated digital sideband-separating downconversion," *Publ. Astron. Soc. Pac.* **122**(889), 326 (2010).
13. A. R. Kerr, S. K. Pan, and J. E. Effland, "Sideband calibration of millimeter-wave receivers," ALMA Memo Series 357 (2001).
14. O. V. Stukach, "Variable attenuator with low phase shift," in *Eur. Conf. Wireless Technol.*, IEEE, pp. 241–244 (2006).
15. T. Kojima et al., "Demonstration of a wideband submillimeter-wave low- noise receiver with 4–21 GHz IF output digitized by a high-speed 32 GSps ADC," *Astron. Astrophys.* **640**, 1–6 (2020).
16. B. Bradford et al., "ROACH-2," CASPER Hardware, 2019, https://github.com/casper-astro/casper-hardware/blob/master/FPGA_Hosts/ROACH2/README.md (2022).

Biographies of the authors are not available.